JACS
JOURNAL OF THE AMERICAN CHEMICAL SOCIETY
Article
pubs.acs.org/JACS

The Proline Enamine Formation Pathway Revisited in Dimethyl Sulfoxide: Rate Constants Determined via NMR

Michael H. Haindl, Johnny Hioe, and Ruth M. Gschwind*

Institut für Organische Chemie, Universität Regensburg, D-93053 Regensburg, Germany

Supporting Information

ABSTRACT: Enamine catalysis is a fundamental activation mode in organocatalysis and can be successfully combined with other catalytic methods, e.g., photocatalysis. Recently, the elusive enamine intermediates were detected, and their stabilization modes were revealed. However, the formation pathway of this central organocatalytic intermediate is still a matter of dispute, and several mechanisms involving iminium and/or oxazolidinone are proposed. Here, the first experimentally determined rate constants and rates of enamine formation are presented using 1D selective exchange spectroscopy (EXSY) buildup curves and initial rate approximation. The trends of the enamine formation rates from *exo*-oxazolidinones and *endo*-oxazolidinones upon variation of the proline and water concentrations as well as the nucelophilic/basic properties of additives are investigated together with isomerization rates of the oxazolidinones. These first kinetic data of enamine formations in combination with theoretical calculations reveal the deprotonation of iminium intermediates as the dominant pathway in dimethyl sulfoxide (DMSO). The dominant enamine formation pathway varies according to the experimental conditions, e.g., the presence and strength of basic additives. The enamine formation is zero-order in proline and oxazolidinones, which excludes the direct deprotonation of oxazolidinones via E2 mechanism. The nucleophilicity of the additives influences only the isomerization rates of the oxazolidinones and not the enamine formation rates, which excludes a nucleophile-assisted anti elimination of oxazolidinones as a major enamine formation pathway.

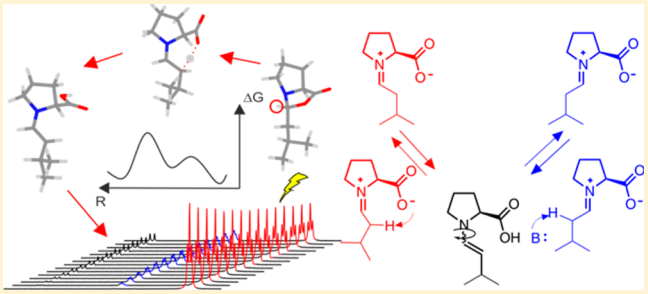

INTRODUCTION

Enamine catalysis is one of the central activation modes in organocatalysis and has proven to be a very powerful method for the enantioselective α-functionalization of carbonyl compounds (e.g., in aldol or Mannich reactions, Michael additions, α-halogenations, α-oxygenations, α-aminations, or domino reactions).[1,2] The primary synthesis applications using proline enamine catalysis were followed by versatile and powerful further developments, e.g., prolinol[3−5] and prolinolether catalysts,[6−9] di-/trienamine[10−12] catalysis, and combinations with photocatalysis.[13−15] Proline oxazolidinones[16] and stabilized enamines[17] were characterized by X-ray crystallography. However, for decades, exclusively oxazolidinones were detected as intermediates by in situ NMR.[18−22] Recently, we observed the elusive proline enamines by in situ NMR[23] and elucidated the stabilization modes of enamines versus oxazolidinones.[23,24] Furthermore, the mechanism of aldol addition versus aldol condensation was investigated,[25] and the formation pathways, conformational preferences, and stereoinduction modes of prolinol and prolinol ether enamines were revealed.[26,27] The formation of imines or iminium ions are generally accepted to proceed via carbinolamines.[28−30] NMR studies on two combinations of aldehydes/ketones with prolinol/prolinolether as catalysts corroborated this intermediate.[31,32] However, the formation pathway of the central proline enamine intermediate is still discussed controversially.

In the most generally accepted mechanism first proposed by Houk and List,[33,34] the enamine is formed directly from the *E*/*Z* zwitterionic iminium via intramolecular deprotonation of one of its α-protons by the carboxylate moiety (Figure 1, pathway I). For this process, Sunoj et al. calculated the lowest energy barrier for *Z*-iminium.[35] In a second pathway, they proposed a water-assisted proton transfer with an amphoteric water molecule protonating the carboxylate and deprotonating the α-proton (Figure 1, II). In this water-assisted pathway, the calculated barriers of *Z*- and *E*-iminium are similar, but both are considerably higher than that in the water-free deprotonation from *Z*-iminium.[35] In a third pathway, they calculated the participation of an external base in the deprotonation step (Figure 1, III). However, with external base the resulting energy barriers are again significantly higher.[35] In the following, all enamine formation pathways via deprotonation from iminium carboxylates herein are referred to as "iminium pathways".

In contrast, in the model of Seebach and Eschenmoser the enamine intermediate is formed directly from the oxazolidinone species.[20] An external base such as an additional proline,

Received: April 1, 2015
Published: September 19, 2015

DOI: 10.1021/jacs.5b03420
J. Am. Chem. Soc. 2015, 137, 12835−12842

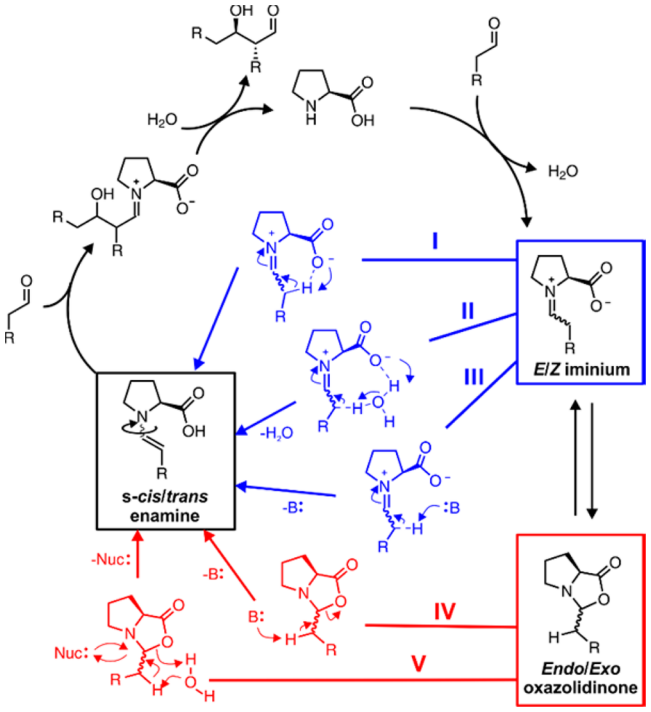

Figure 1. Catalytic cycle of L-proline-catalyzed aldol reactions and proposed enamine formation pathways. Enamine formations via deprotonation of iminium carboxylates are shown in blue (I, intramolecular; II, water-assisted; III, external-base-induced). Deprotonations of oxazolidinones are shown in red (IV, with external base; V, nucleophile-assisted). For the sake of clarity, the *E*-/*Z*-iminium isomers, the diastereomeric *endo*-/*exo*-oxazolidinones, and the *s-cis*-/*s-trans* enamine conformers are presented in condensed forms using waved bonds.

oxazolidinone, or product molecule is proposed to deprotonate the oxazolidinone α-proton and to induce an *anti* E2 elimination (Figure 1, IV). Our own NMR investigations of proline enamine intermediates seemed to corroborate a direct formation of enamines from oxazolidinones providing only exchange spectroscopy (EXSY) cross peaks from oxazolidinones to enamines and none from the aldehydes.[23] In addition, initial studies hinted at a nucleophile-assisted enamine formation from oxazolidinones (Figure 1, V).[31] A nucleophilic ring opening would allow for a water-assisted anti elimination from oxazolidinones and avoid the missing microreversibility of the Seebach–Eschenmoser pathway. Despite the fact that oxazolidinones are also generated via iminium ions, all enamine formation pathways via direct deprotonation from oxazolidinones are referred to herein as "oxazolidinone pathways".

To differentiate between the discussed enamine formation pathways in this work, rates and rate constants of enamine formation were determined experimentally using 1D selective EXSY buildup curves and the initial rate approximation. The presented large number of enamine formation rate constants starting from both *endo*-/*exo*-oxazolidinones, the influence of various additives (L-proline, water, bases, and nucleophiles) on these rate constants, the resulting trends, and the comparison with oxazolidinone isomerization rate constants allow for the first time a detailed experimental insight into the so-far hidden mechanistic relation between enamines and oxazolidinones. These extensive experimental data in combination with theoretical calculations indicate that the enamine is formed via neither E2 elimination nor a nucleophile-assisted pathway from the oxazolidinone but rather via deprotonation of iminium ions.

RESULTS AND DISCUSSION

Model System and Methods. As a model system for this mechanistic study of the enamine formation pathway, the L-proline-catalyzed intermolecular aldol reaction of 3-methylbutanal in dimethyl sulfoxide (DMSO)-d_6 with 100% L-proline was chosen (Figure 2A). In previous studies, we observed for this system the highest enamine concentration in combination with a slow subsequent aldolisation rate. At 300 K, the resulting ^{1}H spectra show well-separated signals of the H1 protons of the enamine as well as of the *exo*- and *endo*-oxazolidinone (Figure 2B). In addition, the quite similar signal intensities of all three

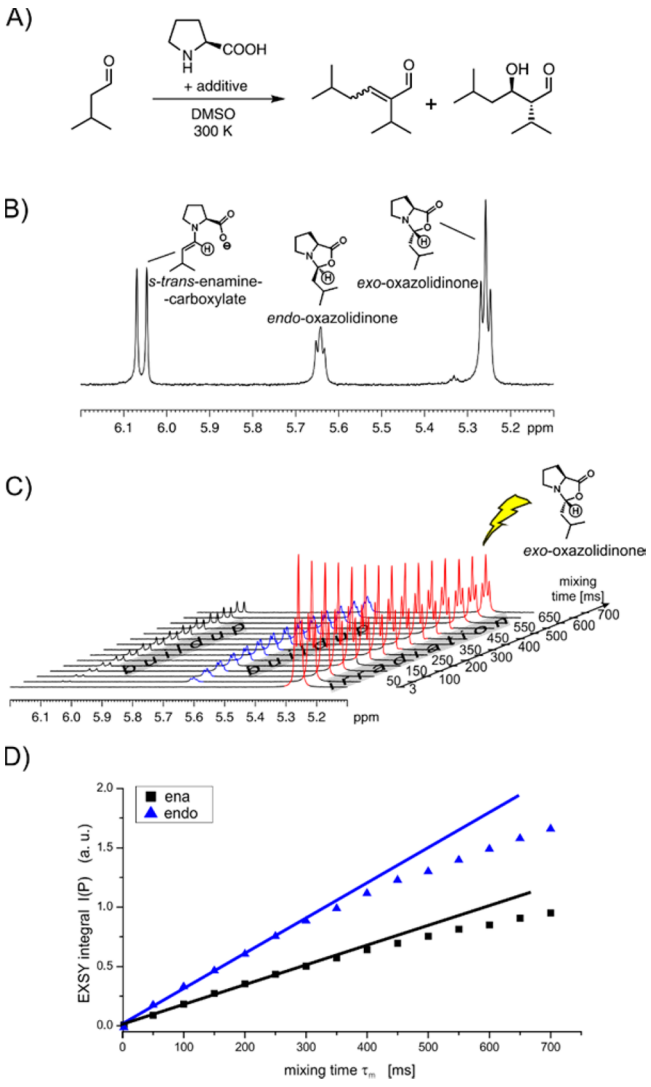

Figure 2. (A) L-Proline-catalyzed self-aldolization of 3-methylbutanal. (B) Section of the ^{1}H spectrum showing well-separated H1 signals (circles) of the enamine and the two oxazolidinones (sample: L-proline (saturated), 3-methylbutanal (50 mM), DABCO (50 mM) in DMSO-d_6 at 300 K). (C) Stack plot of 1D selective EXSY spectra of this sample (irradiation on H1 of *exo*-oxazolidinone, mixing times 3–700 ms). (D) 1D selective EXSY build-up curves (sample without additives); blue (P = *endo*-oxazolidinone) and black (P = enamine) lines represent the initial slopes ($I_{rm}(P)/\tau_m$) used for the initial rate approximation.

DOI: 10.1021/jacs.5b03420
J. Am. Chem. Soc. 2015, 137, 12835–12842

intermediates are ideal for the investigation of chemical exchange between these three species.[36]

In principle, for such a slow exchange on the NMR time scale, magnetization transfer,[37−44] usually called EXSY (exchange spectroscopy), can be used to determine individual rate constants. In 2D EXSY experiments as previously applied in our enamine studies,[23] the complete exchange matrix can be observed qualitatively within one spectrum. However, the quantitative interpretation of EXSY cross peak ratios used in these studies to differentiate between the reaction pathways requires an iminium isomerization being fast compared to all other processes, which is not the case. In addition, multistep transfers similar to spin diffusion in NOESY spectra hampered a reliable quantitative interpretation. (For details, see Supporting Information page S2.) Both problems are circumvented in the present study. The determination of direct reaction rate constants in combination with theoretical calculations avoids the mechanistic prerequisites for the application of the EXSY cross peak ratios. The problem of mixed rates due to multistep transfers can be solved by using the initial rate approximation, similar to the nuclear overhauser effect (NOE).

Within the initial linear buildup of the exchange signal, the slope of this buildup ($I_{\tau m}(P)/\tau_m$; Figure 2D) normalized by the integral of the starting material ($I_0(A)$) is directly correlated to the formation rate of the product (r) divided by the equilibrium concentration of the starting material ([A], Figure 3).[44,45] In

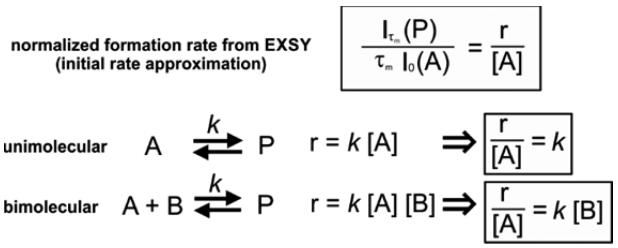

Figure 3. Normalized formation rate from EXSY spectra using the initial rate approximation corresponds to rate constants for unimolecular reactions and rate constants times the concentration of the reaction partner B in the case of bimolecular reactions. r, rate; k, rate constant; τ_m, mixing time; $I_{\tau m}(P)$, EXSY integral of the product signal (e.g., enamine) at τ_m; A, starting material (irradiated species); P, product (buildup species); $I_0(A)$, EXSY integral of the starting material signal (*endo*- or *exo*-oxazolidinone) at $\tau_m = 0$ s; [A] and [B], equilibrium concentrations of A and B.

case the rate-determining step is an unimolecular reaction, the normalized formation rate is equivalent to the rate constant (k). For bimolecular reactions, the normalized formation rate is the rate constant multiplied by the equilibrium concentration of the second reaction partner (k[B], Figure 3). In the following, for the sake of readability, all "normalized rates" are denoted as "rates".

2D EXSY buildup curves are extremely time-consuming and not applicable to one sample in reacting systems. Therefore, in this mechanistic study 1D selective EXSY buildup curves were measured, irradiating selectively the well-separated H1 protons of *endo*-/*exo*-oxazolidinone or enamine. Using very short mixing times, exclusively the irradiated signal is observed (Figure 2C). After a considerable mixing time, the signals of exchanging molecules appear. With the enamine model system described above, considerable amounts of both intermediates, oxazolidinones and enamines, can be detected. To the best of our knowledge, this allows us for the first time to measure EXSY buildup curves between reaction intermediates. Thus, as an unique feature, this study provides rate constants and reaction orders of the rate-limiting steps between intermediate species and not for the whole reaction pathway. In case several reaction steps are involved between the observed intermediates, the rate-limiting step has to be at least 1 order of magnitude slower than all other steps; otherwise, mixed rates are observed.

Previous studies showed that the presence or addition of extra water does not affect the relative ratios of enamine to oxazolidinones but rather reduces their absolute amounts considerably.[23,46,47] Therefore, dry solvents and starting materials were used for all experiments to obtain optimal signal intensities. Nevertheless, a potential participation of water in the formation pathway of enamines cannot be neglected because in all samples at least 1 equiv of water is present, originating from the condensation reaction of aldehyde and proline to oxazolidinones and enamines. In the following, the reaction rate constants from *exo*-oxazolidinone and *endo*-oxazolidinone to the enamine are discussed. (For data regarding the back reaction from enamine to oxazolidinones, see Supporting Information page S10.) First, we investigated the influence of the amount of L-proline and water on the enamine formation rates. In addition, the effect of various additives with varying basic and nucleophilic properties was tested (1,4-diazabicyclo[2.2.2]octane (DABCO), triethylamine (TEA), sodium carbonate, and sodium benzenesulfinate). Acidic additives cannot be applied in this experimental setup because proline enamines are not detectable together with hydrogen bond donors (e.g., in MeOH, no enamine ^{1}H signal can be detected).[23,24]

Participation of Proline, Oxazolidinones, and Water. First, the dependence of the enamine formation rate on the amount of L-proline and water was studied because both are intrinsic components of the reaction. Because the oxazolidinone pathway according to Seebach's proposal (Figure 1, IV) includes the participation of a second proline, oxazolidinone, or product as base (E2 elimination), for this pathway it is expected that the enamine formation rate increases with the proline concentration (Figure 3). In Figure 4A, the experimentally determined rates of enamine formation from both *endo*-oxazolidinone and *exo*-oxazolidinone are presented. At any L-proline or water concentration investigated in the additive-free case, the rate starting from *endo*-oxazolidinone is smaller than that from *exo*-oxazolidinone.

Upon increasing L-proline concentration, the enamine formation is not accelerated but rather remains constant within the experimental error range with a slightly decreasing trend. Similar results were obtained in acetonitrile (Supporting Information page S3). This indicates that the rate-determining step of the enamine formation is zero-order in L-proline (unimolecular; $r/[A] = k$). Our current and previous[23] NMR studies also showed that at higher L-proline concentrations the amount of the two oxazolidinones increases directly proportionally (Supporting Information page S12). Therefore, the rather constant enamine formation rates also exclude the involvement of a second oxazolidinone in the enamine formation pathway (zero-order in oxazolidinone). Thus, Seebach's E2 elimination pathway from oxazolidinone (Figure 1, IV) with either proline or oxazolidinone as external base is not supported by our data. Another possibility would be an aldol product or oxazolidinone product as external base in pathway IV. In this case, an induction period of enamine and

DOI: 10.1021/jacs.5b03420
J. Am. Chem. Soc. 2015, 137, 12835−12842

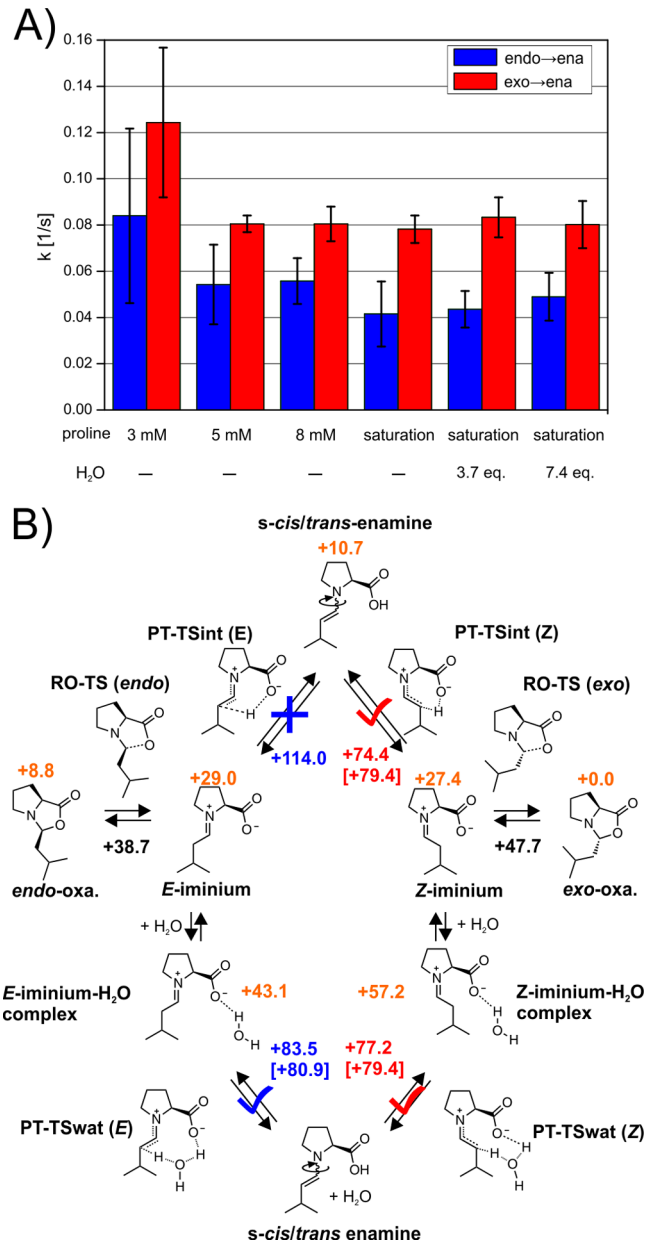

Figure 4. (A) Enamine formation rate constants from *endo*-/*exo*-oxazolidinone dependent on L-proline and external water amount (sample: 50 mM 3-methylbutanal in DMSO-d_6 at 300 K). (B) Summary of calculated free energy barriers $\Delta G^{\ddagger}_{298}$ (kJ mol^{-1}) (ring opening and proton transfer) and thermodynamics stability (orange; referenced to *exo*-oxazolidinone) using a cluster continuum model at CCSD(T)/CBS level of theory in DMSO. For the CBS extrapolation procedure, please refer to the Supporting Information, page S24. The experimental values are shown in brackets.

product formation would be expected from an autocatalytic process. However, in none of our enamine aldol studies[23,25] was such an induction period observed. An adduct of L-proline and oxazolidinone or of two oxazolidinones as reaction intermediates and a subsequent E1 elimination cannot be excluded by these experimental data because the rate-limiting step would be again zero-order in proline. However, theoretical calculations of potential adduct complexes and subsequent E1 eliminations suggest that such processes are extremely unfavorable under synthesis conditions (Supporting Information page S23). Thus, the experiments exclude all enamine formation pathways that are first-order in proline or oxazolidinones under synthesis conditions in DMSO and acetonitrile. Theoretical calculations suggest that pathways starting from proline/oxazolidinone adducts which would be zero-order in proline or oxazolidinone are highly unlikely.

Next, the influence of increasing amounts of water was investigated. The addition of external water does not significantly affect the rates of enamine formation from *exo*/*endo*-oxazolidinone (Figure 4A), indicating again zero-order in water for this step.

In addition, we determined the enamine formation and the oxazolidinone isomerization rate constants for the linear aldehyde 3-phenylpropanal in the additive-free case in DMSO (approximately 0.5 equiv of water). The results are very similar; therefore, the influence of the aldehyde structure is assumed to be minor. (For more details also concerning additional results in acetonitrile, please refer to the Supporting Information, pages S13 and S3.)

Theoretical Calculation of the Enamine Formation. To translate these experimental data into mechanistic enamine formation pathways, various theoretical calculations of potential enamine formation pathways were carried out and compared to the experimentally determined rate constants. The low stability of iminium and enamine has been reported by Houk and Blackmond as the major problem in predicting the experimental reactant/product distribution (oxazolidinone/enamine).[48] In this case, the inclusion of an explicit solvent molecule in the model is becoming compulsory to cover the missing interaction between solvent and solute. This is also confirmed by our present study. At least one solvent molecule is needed to predict the enamine/oxazolidinone ratio and, as shown later, the barrier heights correctly. (For the data regarding the discussion of solvent molecule and the simulation without explicit solvent, refer to Supporting Information page S19.) Therefore, calculations with a cluster continuum model[49−51] were carried out.

The contribution of additional L-proline or oxazolidinone in bimolecular mechanisms was excluded experimentally and therefore omitted in the theoretical calculations. Our previous EXSY studies suggested a nucleophile-assisted enamine formation from oxazolidinone (Figure 1, V).[31] Therefore, we tried to simulate the ring opening of oxazolidinone by DABCO as nucleophile/base together with a simultaneous α-proton transfer to the carboxylate group and a subsequent dissociation of the nucleophile. Furthermore, we also tried to abstract the α-proton by DABCO and to locate an E2 elimination transition state as proposed by Seebach (Figure 1, IV). However, all attempts to locate any transition state lead to either iminium−nucleophile adducts or oxazolidinones. The only transition state found stems from the addition of a nucleophile to the iminium ion after the ring opening of the oxazolidinone facilitating the *E*-/*Z*-iminium isomerization. As shown later, this is corroborated by the experimental data, which show that nucleophiles accelerate the *exo*-/*endo*-oxazolidinone exchange rate but not the enamine formation rates. (See below and Supporting Information on page S5.) Therefore, the Houk−List pathway was recalculated on a refined level of theory (Figure 4B) and compared to the experimental rate constants (Figure 4A).

Our calculations showed that in the Houk−List pathway the *endo*-oxazolidinone is exclusively connected with the *E*-iminium and the *exo*-oxazolidinone with the *Z*-iminium (Figure 4B) which is consistent with previous calculations of Sharma and Sunoj.[35] Without water, the activation barrier of the subsequent

DOI: 10.1021/jacs.5b03420
J. Am. Chem. Soc. 2015, 137, 12835−12842

internal deprotonation step from *Z*-iminium to enamine is calculated to be +74.4 kJ mol^{-1} compared to +114 kJ mol^{-1} when starting from *E*-iminium. Rather, this higher activation barrier (by approximately 40 kJ mol^{-1}) from *E*-iminium is due to the unfavorable geometry of the transition state. In case of a water-assisted deprotonation step, the situation changes. Now the activation barrier starting from an *E*-iminium water complex is considerably lower (+83.5 kJ mol^{-1}) than in the water-free pathway. In the case of deprotonation from *Z*-iminium via water, the barrier is only marginally higher (+77.2 kJ mol^{-1}) than that in the internal deprotonation. Qualitatively, these two preferred pathways are in agreement with the previous calculations of Sunoj and Sharma using a smaller model in the gas phase and a lower level of theory (ΔG_{298} B3LYP/6-31G**).[35] As expected, the change of phase (gas phase to condensed phase) and theoretical model in our present work led to three significant differences. First, the ring-opening barriers in the study of Sunoj and Sharma are rather high (+53.6 kJ mol^{-1} (*endo*) and + 73.6 kJ mol^{-1} (*exo*)) compared to ours (+38.7 kJ mol^{-1} (*endo*) and + 47.4 kJ mol^{-1} (*exo*)) most probably because of the fact that they did not include solvent effects in their calculation. (See Supporting Information page S20 for further discussion.) Second, the energy barrier for the water-assisted deprotonation from *E*- and *Z*-iminium are very similar in the gas phase at the DFT level of theory (differing by 2.5 kJ mol^{-1}) and quite low (+53.6 kJ mol^{-1} for *E*-iminium and +51.1 kJ mol^{-1} for *Z*-iminium). In our calculation, the difference amounts to 6.3 kJ mol^{-1}, and the barriers are significantly higher (Figure 4B). Again, this is an artifact from the gas-phase calculation. As stated in their supporting information, the solvent correction in acetonitrile leads to an increase of barrier height by ∼40 kJ mol^{-1} for both *E*-/*Z*-iminium−enamine transition states, which would approach our predicted values. Third, although it does not have a significant impact, we also notice here that the energy barrier difference between *Z*-iminium and *E*-iminium for the water-free pathway is slightly higher (+54.0 kJ mol^{-1}) in their calculation than in our present data (+39.6 kJ mol^{-1}).

Next, the experimentally determined rate constants were converted into activation barriers and compared to our theoretical calculation. (For details, see Supporting Information page S24.) The activation barriers for the ring-opening processes are at least 20 kJ mol^{-1} lower than those of the deprotonation processes from iminium ions to enamines. This translates to several orders of magnitude difference in rate constants. Hence, the experimental rate constants correspond exclusively to the barrier of the deprotonation process. The experimental conditions being closest to those of our theoretical calculations (one L-proline, one aldehyde, and one water molecule) are those at saturation with L-proline and without additional water. For this sample, an activation barrier of +79.4 kJ mol^{-1} is experimentally determined starting from *Z*-iminium and of +80.9 kJ mol^{-1} starting from *E*-iminium. This is qualitatively and quantitatively in good agreement with our theoretical data for the internal deprotonation from *Z*-iminium as well as with that of the water-assisted deprotonation from both *E*- and *Z*-iminium (numbers in Figure 4B). Considering the absence and the presence of water in the three pathways of the lowest transition states, at first glance one would expect that increasing amounts of water would affect these pathways differently. However, the experimental data show that the rate-determining steps of all pathways are zero-order in water. (See Figure 4A and discussion above.) That is directly obvious for the water free pathway starting from *Z*-iminium. For the water-assisted pathways starting from *E*- and *Z*-iminium, the theoretical data suggest the formation of an intermediate consisting of iminium and water, followed by a deprotonation step that is zero-order in water because the reference iminium intermediate already includes water. Thus, from the experimental data the assistance of water cannot be directly deduced, but the measured rate constants are in agreement with the most preferred pathways from theoretical calculations.

A summary of the active enamine formation pathways without additives is shown in Figure 5. Without additives, the dominant process is the proton transfer from *Z*-iminium, which is connected with the *exo*-oxazolidinone. The water-assisted deprotonation of *E*-iminium is also observed but at a slower rate.

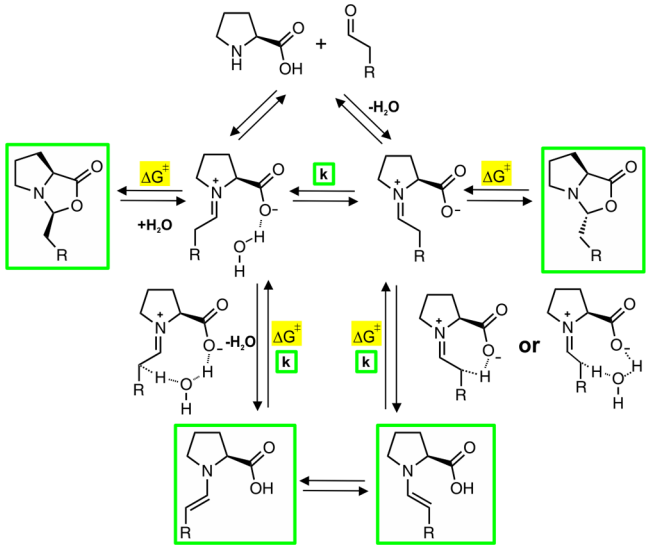

Figure 5. Summary of enamine formation without additives for R = C_3H_7 and phenyl in DMSO. The experimentally measured intermediates and rate constants are highlighted in green, and the calculated activation barriers are highlighted in yellow.

Influence of Basic Additives. Next, the influence of basic additives (DABCO, TEA, sodium carbonate and sodium benzenesulfinate) was measured to elucidate a potential correlation between enamine formation rates and basicity. However, not all pK_{aH} values of the additives are known in DMSO. Therefore, an internal basicity scale was created. Our previous enamine study with basic additives showed that the amount of enamine increases at the expense of oxazolidinone with increasing basicity of the additive.[24] Therefore, the ratio of enamine to total intermediate concentration was used as a measure for the internal basicity in DMSO. The results showed an increasing basicity from sodium benzenesulfinate over TEA and DABCO to sodium carbonate. (For data and details, see Supporting Information page S4.)

In contrast to the measurements with varying water and proline concentrations, the rate of enamine formation is dependent on the concentration of the additives. This indicates that the rate-limiting deprotonation step is bimolecular (participation of starting molecule and base). (See Figure 3 bimolecular and Supporting Information page S16 for details.) In Figure 6A, the rate constants for the additive-free sample and those with TEA are given. Upon addition of TEA, the rate constant of enamine formation increases drastically, and the

DOI: 10.1021/jacs.5b03420
J. Am. Chem. Soc. 2015, 137, 12835−12842

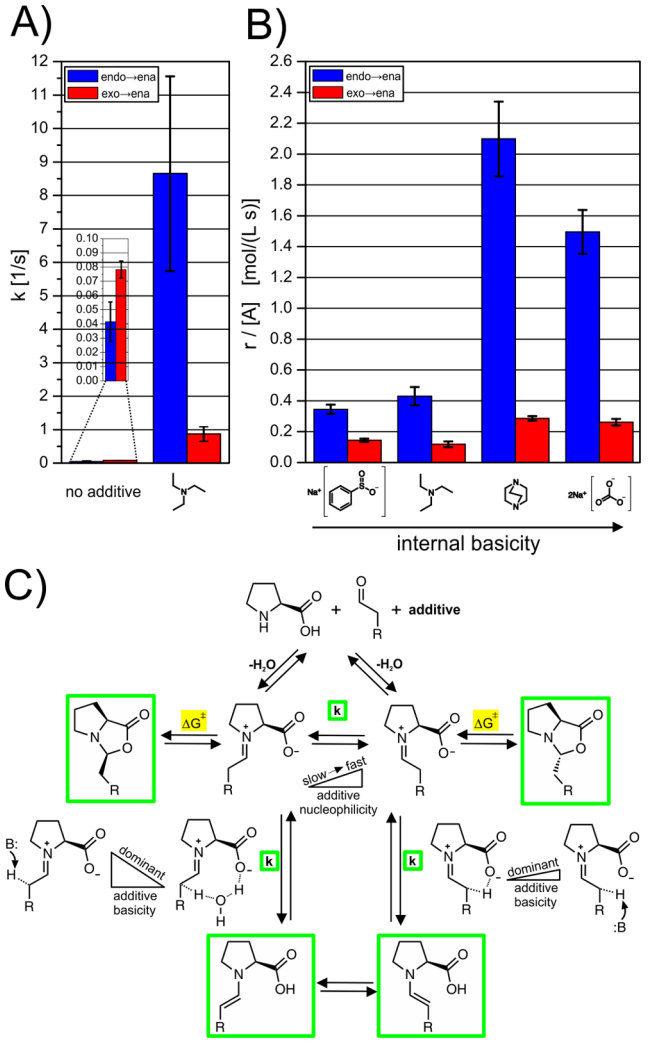

Figure 6. (A) The enamine formation rate constants drastically increase with the addition of the basic additive TEA, whereas the relative rate constants from *endo*- and *exo*-oxazolidinone invert. (B) The enamine formation rates increase with the basicity of the additives. Additives invert the relative rates from *endo*- and *exo*-oxazolidinones and accelerate especially those from *endo*-oxazolidinone (sample: L-proline (saturated), 3-methylbutanal (50 mM), additive (50 mM, for sodium carbonate: saturated solution) in DMSO-d_6 at 300 K). (C) Summary of enamine formation pathways in the presence of additives. Basic additives accelerate strongly the deprotonation from *E*-iminium but only slightly that from *Z*-iminium. Nucleophiles accelerate the *E*-/*Z*-iminium isomerization.

relative order of enamine formation rate constants starting from *endo*- and *exo*-oxazolidinones are inverted. In Figure 6B, the normalized rates for all additives (50 mM) as well as their correlation with the internal basicity scale are presented. All additives show high enamine formation rates starting from *endo*-oxazolidinone. In contrast, the rates starting from *exo*-oxazolidinone are much lower. Overall, both trends follow the relative internal basicity of the additives but with different slopes. One exception is sodium carbonate, which shows a considerably lower enamine formation rate from *endo*-oxazolidinone than from DABCO.[52] Another striking change is the general switch of the relative rate constants and rates starting from *endo*-oxazolidinones and *exo*-oxazolidinones, respectively. Without basic/nucleophilic additives, the rate constants from *endo*-oxazolidinone are smaller than those from *exo*-oxazolidinone (Figures 4A and 6A, first entry). With basic/nucleophilic additives, the situation is inverted; in all cases, the rate constants (Figure 6A, second entry) and rates (Figure 6B) from *endo*-oxazolidinone are significantly larger than those from *exo*-oxazolidinone. These experimental data fit to the theoretical calculations shown in Figure 4B with additional pathways of *E*- and *Z*-iminium deprotonation by external bases (Figure 6C). The rapid increase of the rate constant and rates from *endo*-oxazolidinone indicates that external bases can easily deprotonate the *E*-iminium. For *exo*-oxazolidinone, the slope with increasing basicity is significantly lower, which can be explained by steric hindrance and electrostatic repulsion between the base and the carboxylate moiety in the case of the *Z*-iminium.

External bases potentially could also deprotonate the oxazolidinones directly as previously proposed by Seebach et al.[20] *endo*-Oxazolidinones are well-known to be sterically more congested than the corresponding *exo*-oxazolidinones. However, for the proposed E2 *anti* elimination not the internal steric hindrance but rather the steric hindrance of one of the two α protons in anti conformation to the oxazolidinone CO bond has to be considered. Nevertheless, the structures of *endo*- and *exo*-oxazolidinones do not exhibit significant differences in the steric hindrance of these α-protons (Supporting Information page S12). Thus, steric arguments of the oxazolidinones cannot explain the very different behavior of enamine formation rates from *endo*- and *exo*-oxazolidinones with increasing basicity. This excludes the direct deprotonation of oxazolidinones (Figure 1, IV) as a major pathway in the presence of bases.

Influence of Nucleophilic Additives. Next, a correlation of the enamine formation rates toward Mayr's nucleophilicity scale[53] was considered. Benzenesulfinate shows hardly any basicity, but it is a very strong S nucleophile (*N* value of 19.6 in DMSO). For the tertiary amine bases DABCO and TEA, only *N* values in acetonitrile are available, which are considerably lower (18.8 and 17.1, respectively). The experimental enamine formation rates from both oxazolidinones are significantly lower for benzenesulfinate than for DABCO (Figure 6B), which supports the discussion above, i.e., that not the nucleophilicity but rather the basicity of the additive is crucial for the enamine formation rate constants. These results exclude pathway V, i.e., a nucleophile-assisted anti elimination of oxazolidinones leading to enamines as a major formation pathway in DMSO.

However, another effect of additional nucleophiles was observed experimentally: the accelerated exchange between *exo*-oxazolidinones and *endo*-oxazolidinones. (For details, see Supporting Information page S5.)

■ CONCLUSIONS

Detailed experimental enamine formation rate constants and rates from both *endo*-oxazolidinone and *exo*-oxazolidinone are presented. Their dependence on the addition of L-proline, water, and additives with various basic and nucleophilic properties was investigated. The mechanistic interpretation of these data is confirmed by higher level theoretical calculations of the enamine formation pathway. First, the enamine formation is zero-order in proline and oxazolidinones, which excludes the Seebach pathway V proposing an E2 deprotonation of oxazolidinones. Prereacting oxazolidinone−proline complexes undergoing E1 elimination cannot be excluded experimentally but are highly unlikely according to theoretical calculations. Without additives, the fastest process is the proton transfer from *Z*-iminium (pathways I + II from *exo*-

DOI: 10.1021/jacs.5b03420
J. Am. Chem. Soc. 2015, 137, 12835−12842

oxazolidinone), whereas the deprotonation of *E*-iminium follows the water-assisted pathway II (from *endo*-oxazolidinone) at a slower rate. Basic additives change the situation considerably. Now, the deprotonation via an external base is preferred (pathway III). The acceleration of the enamine formation is significantly more pronounced for *E*-iminium (from *endo*-oxazolidinone) than for *Z*-iminium (from *exo*-oxazolidinone) and correlates to the basicity of the additive. These trends are in agreement with the steric and electronic properties of the iminium intermediates (pathways I, II, and III) but not with those of the oxazolidinones (exclusion of pathway IV with basic additives). The nucleophilicity of the additives influences only the isomerization rates of the two oxazolidinones but not the enamine formation rates. This excludes a nucleophile-assisted anti elimination of oxazolidinones as a major enamine formation pathway (pathway V). Thus, the first kinetic data of enamine formation together with theoretical calculations reveal that enamines are most likely formed via deprotonation of iminium intermediates (Houk–List pathway) in DMSO. The dominant pathway varies according to the experimental conditions, e.g., the presence and strength of a basic additive.

COMPUTATIONAL DETAILS

The geometry of all systems was optimized in the gas phase at TPSS-D3/aug-SVP level of theory (Ahlrichs SVP[54,55] augmented with diffuse function from aug-cc-VDZ[56,57]) corrected with empirical dispersion from Grimme.[58,59] Harmonic vibrational frequency and thermochemical correction were carried out at the geometry optimization level. Single point calculations were done at domain-based local pair natural orbital (DLPNO)–coupled cluster singles doubles with triples from perturbation theory (CCSD(T))/complete basis set (CBS)[60,61] using density fitting (Split-RI-J) and seminumerical approximation for the exchange term (RIJCOSX) for the reference wave function[62−64] and DLPNO approximation for the post-HF part. Two-points extrapolation technique to approach CBS was used using def2-QZVPP and def2-TZVPP basis sets as implemented in ORCA.[65,66] The solvent correction ΔG_{solv} was calculated at TPSS-D3/aug-TZVP (Ahlrichs TZVP[54,55] augmented with diffuse function from aug-cc-VDZ[56,57]) using COSMO model in DMSO and subsequently added to the single-point energy.[67,68] The software used was ORCA-3.0.3. The extrapolation procedure, energies, and structures are provided in the Supporting Information.

ASSOCIATED CONTENT

Supporting Information

The Supporting Information is available free of charge on the ACS Publications website at DOI: 10.1021/jacs.5b03420.

Details about the experimental setup, the theoretical calculations, the calculation of rate constants, and additional NMR and theoretical data. (PDF)

AUTHOR INFORMATION

Corresponding Author

*ruth.gschwind@ur.de

Notes

The authors declare no competing financial interest.

ACKNOWLEDGMENTS

We gratefully acknowledge financial support from the DFG, grant GS 13/4-1. We thank Dr. Markus Schmid for the initial NMR investigations leading to the proposal of the nucleophile-assisted deprotonation pathway from oxazolidinones. We also thank the Leibniz Rechenzentrum for providing computational facility.

REFERENCES

(1) Pihko, P. M.; Majander, I.; Erkkilä, A. *Top. Curr. Chem.* **2009**, *291*, 29.
(2) List, B. *Synlett* **2001**, *2001*, 1675.
(3) Zhong, G.; Fan, J.; Barbas, C. F. *Tetrahedron Lett.* **2004**, *45*, 5681.
(4) Hayashi, Y.; Itoh, T.; Aratake, S.; Ishikawa, H. *Angew. Chem., Int. Ed.* **2008**, *47*, 2082.
(5) Enders, D.; Chow, S. *Eur. J. Org. Chem.* **2006**, *2006*, 4578.
(6) Hayashi, Y.; Gotoh, H.; Hayashi, T.; Shoji, M. *Angew. Chem., Int. Ed.* **2005**, *44*, 4212.
(7) Chi, Y.; Gellman, S. H. *Org. Lett.* **2005**, *7*, 4253.
(8) Marigo, M.; Wabnitz, T. C.; Fielenbach, D.; Jørgensen, K. A. *Angew. Chem., Int. Ed.* **2005**, *44*, 794.
(9) Palomo, C.; Mielgo, A. *Angew. Chem., Int. Ed.* **2006**, *45*, 7876.
(10) Ramachary, D. B.; Reddy, Y. V. *Eur. J. Org. Chem.* **2012**, *2012*, 865.
(11) Kumar, I.; Ramaraju, P.; Mir, N. A. *Org. Biomol. Chem.* **2013**, *11*, 709.
(12) Dieckmann, A.; Breugst, M.; Houk, K. N. *J. Am. Chem. Soc.* **2013**, *135*, 3237.
(13) Nicewicz, D. A.; MacMillan, D. W. C. *Science* **2008**, *322*, 77.
(14) Neumann, M.; Füldner, S.; König, B.; Zeitler, K. *Angew. Chem., Int. Ed.* **2011**, *50*, 951.
(15) Pirnot, M. T.; Rankic, D. A.; Martin, D. B. C.; MacMillan, D. W. C. *Science* **2013**, *339*, 1593.
(16) Seebach, D.; Boes, M.; Naef, R.; Schweizer, W. B. *J. Am. Chem. Soc.* **1983**, *105*, 5390.
(17) Bock, D. A.; Lehmann, C. W.; List, B. *Proc. Natl. Acad. Sci. U. S. A.* **2010**, *107*, 20636.
(18) List, B.; Hoang, L.; Martin, H. J. *Proc. Natl. Acad. Sci. U. S. A.* **2004**, *101*, 5839.
(19) Iwamura, H.; Wells, D. H.; Mathew, S. P.; Klussmann, M.; Armstrong, A.; Blackmond, D. G. *J. Am. Chem. Soc.* **2004**, *126*, 16312.
(20) Seebach, D.; Beck, A. K.; Badine, D. M.; Limbach, M.; Eschenmoser, A.; Treasurywala, A. M.; Hobi, R.; Prikoszovich, W.; Linder, B. *Helv. Chim. Acta* **2007**, *90*, 425.
(21) Isart, C.; Burés, J.; Vilarrasa, J. *Tetrahedron Lett.* **2008**, *49*, 5414.
(22) Orsini, F.; Pelizzoni, F.; Forte, M.; Sisti, M.; Bombieri, G.; Benetollo, F. *J. Heterocycl. Chem.* **1989**, *26*, 837.
(23) Schmid, M. B.; Zeitler, K.; Gschwind, R. M. *Angew. Chem., Int. Ed.* **2010**, *49*, 4997.
(24) Schmid, M. B.; Zeitler, K.; Gschwind, R. M. *Chem. - Eur. J.* **2012**, *18*, 3362.
(25) Schmid, M. B.; Zeitler, K.; Gschwind, R. M. *J. Org. Chem.* **2011**, *76*, 3005.
(26) Schmid, M. B.; Zeitler, K.; Gschwind, R. M. *J. Am. Chem. Soc.* **2011**, *133*, 7065.
(27) Schmid, M. B.; Zeitler, K.; Gschwind, R. M. *Chem. Sci.* **2011**, *2*, 1793.
(28) Bruice, P. Y.; Bruice, T. C. *J. Am. Chem. Soc.* **1978**, *100*, 4793.
(29) Bruice, P. Y. *J. Am. Chem. Soc.* **1989**, *111*, 962.
(30) Bruice, P. Y. *J. Am. Chem. Soc.* **1990**, *112*, 7361.
(31) Schmid, M. B. Ph.D. Thesis, University of Regensburg, Regensburg-Germany, January 2011.
(32) Seegerer, A. Master Thesis, University of Regensburg, Regensburg-Germany, September 2014.
(33) Bahmanyar, S.; Houk, K. N.; Martin, H. J.; List, B. *J. Am. Chem. Soc.* **2003**, *125*, 2475.
(34) List, B.; Lerner, R. A.; Barbas, C. F. *J. Am. Chem. Soc.* **2000**, *122*, 2395.

DOI: 10.1021/jacs.5b03420
J. Am. Chem. Soc. 2015, 137, 12835–12842

(35) Sharma, A. K.; Sunoj, R. B. *Angew. Chem., Int. Ed.* **2010**, *49*, 6373.
(36) So far no iminium can be detected in our system. Therefore, only oxazolinones and enamine can be directly investigated.
(37) Orrell, K. G.; Šik, V.; Stephenson, D. *Prog. Nucl. Magn. Reson. Spectrosc.* **1990**, *22*, 141.
(38) Campbell, I. D.; Dobson, C. M.; Ratcliffe, R. G.; Williams, R. J. P. *J. Magn. Reson.* **1978**, *29*, 397.
(39) Forsén, S.; Hoffman, R. A. *J. Chem. Phys.* **1963**, *39*, 2892.
(40) Perrin, C. L.; Johnston, E. R. *J. Magn. Reson.* **1979**, *33*, 619.
(41) Günther, H. *NMR Spectroscopy*, 3rd ed.; Wiley-VCH: Weinheim, 2013.
(42) Bain, A. D. *Prog. Nucl. Magn. Reson. Spectrosc.* **2003**, *43*, 63.
(43) Aski, S. N.; Takacs, Z.; Kowalewski. *Magn. Reson. Chem.* **2008**, *46*, 1135.
(44) Perrin, C. L.; Dwyer, T. J. *Chem. Rev.* **1990**, *90*, 935.
(45) Kumar, A.; Wagner, G.; Ernst, R. R.; Wuethrich, K. *J. Am. Chem. Soc.* **1981**, *103*, 3654.
(46) Nyberg, A. I.; Usano, A.; Pihko, P. M. *Synlett* **2004**, *11*, 1891.
(47) Pihko, P. M.; Laurikainen, K. M.; Usano, A.; Nyberg, A. I.; Kaavi, J. A. *Tetrahedron* **2006**, *62*, 317.
(48) Hein, J. E.; Burés, J.; Lam, Y.; Hughes, M.; Houk, K. N.; Armstrong, A.; Blackmond, D. G. *Org. Lett.* **2011**, *13*, 5644.
(49) Bryantsev, V. S.; Diallo, M. S.; Goddard, W. A., III *J. Phys. Chem. B* **2008**, *112*, 9709.
(50) Pliego, J. R.; Riveros, J. M. *J. Phys. Chem. A* **2001**, *105*, 7241.
(51) Thar, J.; Zahn, S.; Kirchner, B. *J. Phys. Chem. B* **2008**, *112*, 1456.
(52) Most probably this is due to the bad solubility of sodium carbonate in DMSO. The amount of sodium carbonate dissolved is much lower than that in the other additive samples. Therefore, the enamine formation rates are not as high as expected from its internal basicity.
(53) Baidya, M.; Kobayashi, S.; Mayr, H. *J. Am. Chem. Soc.* **2010**, *132*, 4796.
(54) Schäfer, A.; Huber, C.; Ahlrichs, R. *J. Chem. Phys.* **1994**, *100*, 5829.
(55) Schäfer, A.; Horn, H.; Ahlrichs, R. *J. Chem. Phys.* **1992**, *97*, 2571.
(56) Kendall, R. A., Jr.; Dunning, T. H.; Harrison, R. *J. Chem. Phys.* **1992**, *96*, 6796.
(57) Woon, D. E.; Dunning, T. H. *J. Chem. Phys.* **1993**, *98*, 1358.
(58) Tao, J.; Perdew, J. P.; Staroverov, V. N.; Scuseria, G. E. *Phys. Rev. Lett.* **2003**, *91*, 146401.
(59) Grimme, S.; Ehrlich, S.; Goerigk, L. *J. Comput. Chem.* **2011**, *32*, 1456.
(60) Riplinger, C.; Sandhoefer, B.; Hansen, A.; Neese, F. *J. Chem. Phys.* **2013**, *139*, 134101.
(61) Riplinger, C.; Neese, F. *J. Chem. Phys.* **2013**, *138*, 034106.
(62) Neese, F.; Wennmohs, F.; Hansen, A.; Becker, U. *Chem. Phys.* **2009**, *356*, 98.
(63) Neese, F. *J. Comput. Chem.* **2003**, *24*, 1740.
(64) Izsák, R.; Neese, F. *J. Chem. Phys.* **2011**, *135*, 144105.
(65) Weigend, F.; Furche, F.; Ahlrichs, R. *J. Chem. Phys.* **2003**, *119*, 12753.
(66) Neese, F. *Wiley Interdiscip. Rev. Comput. Mol. Sci.* **2012**, *2*, 73.
(67) Klamt, A.; Schüürmann, G. *J. Chem. Soc., Perkin Trans. 2* **1993**, 799.
(68) Klamt, A. *Wiley Interdisciplinary Reviews: Computational Molecular Science* **2011**, *1*, 699.

DOI: 10.1021/jacs.5b03420
J. Am. Chem. Soc. 2015, 137, 12835−12842